State-of-Charge Estimation Using Triple Forgetting Factor Adaptive Extended Kalman Filter for Battery Energy Storage Systems in Electric Bus Applications

State-of-Charge Estimation Using Triple Forgetting Factor Adaptive Extended Kalman Filter for Battery Energy Storage Systems in Electric Bus Applications

Mena S. ElMenshawy*, Ahmed M. Massoud*, *Senior Member, IEEE*, Paolo Guglielmi**, *Member, IEEE*

Department of Electrical Engineering, Qatar University, Doha, Qatar; Department of Energy, Politecnico di Torino, Torino, Italy*
malmenshawy@qu.edu.qa, ahmed.massoud@qu.edu.qa, paolo.guglielmi@polito.it

Correspondence: malmenshawy@qu.edu.qa

***Abstract*— The transport sector has been moving towards electrification due to the significant advancement in E-mobility technology. This prioritizes reliable and safe battery energy storage system (BESS) operation. Therefore, accurate battery State-of-Charge (SoC) estimation is essential in effectively monitoring and controlling the BESS stability. Many studies have been conducted to estimate the BESS SoC and improve the estimation accuracy. Nevertheless, considering system complexity and computational efforts, the suggested SoC estimate techniques fall short of providing optimal filtering performance with high noise levels. In this regard, this paper introduces SoC estimation using the Triple Forgetting Factor Adaptive Extended Kalman Filter (TFF-AEKF) to provide better SoC estimation accuracy and faster convergence considering the high measurement noise levels and environmental circumstances encountered by the operation of EBs. The performance of the proposed TFF-AEKF is evaluated and compared to the conventional AEKF and the Dual Forgetting Factor AEKF (DFF-AEKF), considering low and high measurement noise levels. It has been validated that the proposed algorithm can provide faster convergence and better accuracy when considering a high measurement noise level. In addition, the three filters are evaluated using four performance indicators, namely, Maximum Absolute Error (MaxAE), Mean Absolute Error (MAE), Root Mean Square Error (RMSE), and convergence time. It is concluded that the presented method offers faster convergence and lower error. Results have demonstrated that the proposed algorithm provides an RMSE of 0.3%, an MAE of 0.01%, and a MaxAE of 1.7% for SoC estimation.**

***Index Terms*— Electric Buses, Battery Energy Storage System, State of Charge, Triple Forgetting Factor Adaptive Extended Kalman Filter.**

1. INTRODUCTION

With the expansion of E-mobility technology, the transport sector has been moving towards zero-emission transportation, where electrification is highly concerned. There is tremendous interest worldwide in replacing gasoline-powered vehicles with low-carbon mobility or E-mobility technologies, specifically Electric Buses (EBs) [1]. Therefore, a completely safe operation is essential to ensure customer satisfaction. However, the EB batteries, such as Li-ion batteries, are the primary technical bottleneck that may affect the proliferation of the EBs. A Li-ion battery is favored for transport systems due to its high energy density, low self-discharge rate, reduced charging time, reduced weight and size, and wide operating temperature range [2].

It is essential to develop an efficient battery management system (BMS) that ensures batteries' lifetime extension, cost reduction, energy management optimization, safeguarding, and safe application of batteries in EBs. However, EBs are influenced by the driving loads and operating conditions, making real-time accurate state estimation challenging. For example, among the essential functions of the BMS, the State-of-Charge (SoC) serves as a critical indicator. It supports regulating charging and discharging limits, ensures safe and reliable battery operation, and helps alleviate driver range anxiety. Thus, a key task in promoting the widespread adoption of EBs is ensuring accurate SoC estimation. However, SoC cannot be directly measured/ assessed through sensor measurement or a particular instrument. Several variables, including current, voltage, and temperature, are measured to estimate the battery's SoC. In addition, the SoC estimation process is influenced by several factors, including temperature, discharge rate, number of cycles, voltage, and noise, making real-time SOC estimation more challenging. Hence, a proper and accurate battery model should be established for SoC estimation to effectively reflect the relation between the battery's model parameters and its internal state [3].

EB applications are usually incorporated with multiple electric noise sources. These noise sources include the motor and the generated electromagnetic interference during inverter operations resulting from the switching operations, which affect the nearby battery sensors. Noise is also produced by other power electronic devices and their cooling fans. Moreover, battery monitoring can be influenced by regenerative braking systems due to the noise produced during the rapid switching of power. Furthermore, battery sensors may also be influenced by the noise produced by the auxiliary systems, such as HVAC systems, lighting, and onboard electronics [4], [5].

Accurate SoC estimation guarantees a safe and reliable operation of the EB, improves and extends the battery's lifetime, and reduces the EB life cycle costs. However, due to the nonlinearity of the battery model and measurements, the SoC estimation is a challenging task and is formulated as a non-linear parameter estimation problem. In addition, considering the inconsistent characteristics of each cell makes the SoC estimation more challenging. Moreover, the temperature, aging,

and charging process highly influence the battery performance.

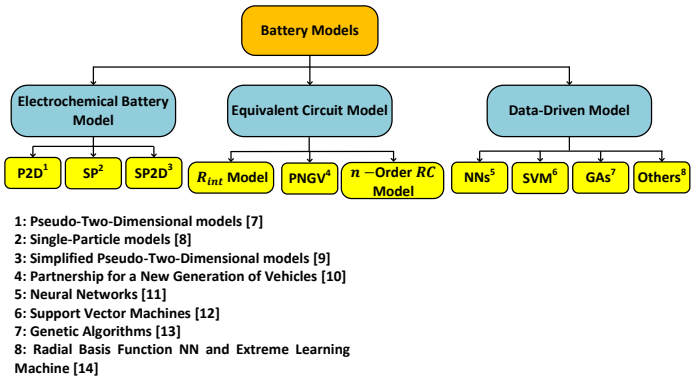

Fig. 1. Battery model classification [6]-[14].

The established battery models can be classified into three main categories: electrochemical battery models, equivalent circuit models, and data-driven models [3]. Fig. 1 presents the battery model classification. The electrochemical model illustrates battery behavior through the electrochemical process, the electrolyte concentration, and the anode and cathode size, providing high accuracy. However, it adds complexity and additional computational efforts due to the complex partial differential equations and the significant number of parameters involved in the battery model.

Data-driven battery models use extensive data to map the non-linearity between the input and the output. Such models are typically established by machine learning approaches. Extensive data are required to train the model and present the battery's behavior, consuming more time and adding extra computational effort. The model's accuracy is highly dependent on the quantity and quality of the trained data.

Among the available battery models, the equivalent circuit model (ECM) is a favored choice since it compromises model accuracy, computational complexity, and simple structure and configuration. The ECM can be established using the R_{int} model, partnership for a new generation of vehicles (PNGV) model, which stands for the partnership for a new generation of vehicles, n −order RC model, and Thevenin model. In the electrical equivalent circuit model, the electric circuit component's interconnections and values corresponding to the electrochemical impedance spectroscopy (EIS) data are utilized to explain the battery's aging mechanism. However, when employing other battery types, the model should re-consider the behavior of the new battery type. In addition, the SoC estimation accuracy is highly dependent on the model's accuracy. The equivalent circuit model presents the battery dynamics in a less complex way through fewer states and dynamics. Thus, such a model is more favorable for fast SoC estimation.

The R_{int} model is the simplest among the models and mainly involves a DC source and an internal resistance. However, it is considered an ideal model and does not consider the battery's internal state, which makes this model impractical. In the PNGV model, the discharging process is considered, while the charging process circuit model is not considered. On the other hand, the n −order RC model can present the relation between the battery's internal parameters and the current or the temperature. Nevertheless, the model complexity increases as the order increases, adding extra burden on the microcontroller. Consequently, the second-order RC model is usually selected since it can provide less complexity and good accuracy through a concise structure and configuration. Therefore, in this work, the second-order RC model is considered a balanced approach to optimizing the system's accuracy and complexity.

Many studies have been conducted to estimate the BESS SoC and increase the estimation accuracy [2], [15]-[50]. Fig. 2 presents a tree diagram for the SoC estimation methods. SoC

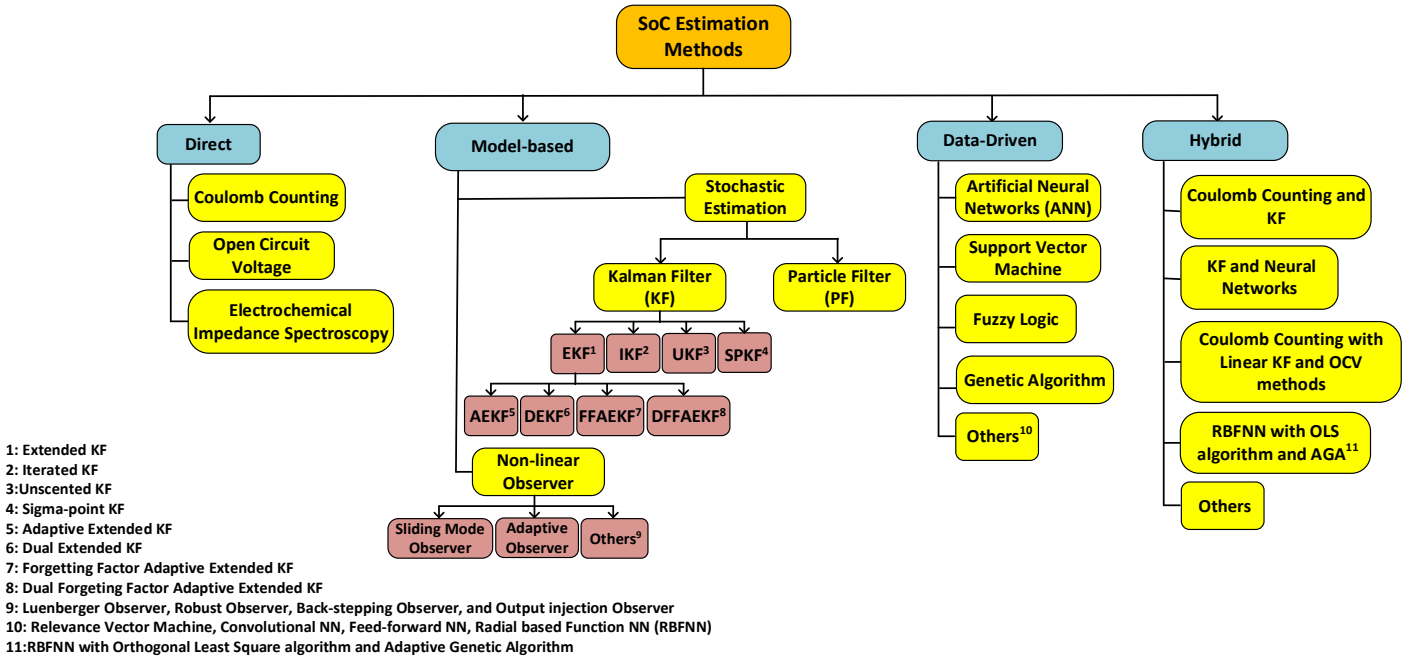

Fig. 2. SoC estimation methods.

Table 1. Comparison between SoC estimation methods

SoC Estimation Methods	Advantages	Disadvantages
Direct Methods	✓ Provide less complexity ✓ Require low computational load ✓ Simple and easy to implement	× Difficult implementation in practical applications × Open-loop control × Sensitive to the measurements noise and initial SoC condition × Not applicable with battery cells that have flat OCV-SoC curves as well as dynamic estimation
Model-based Methods	✓ Provide good dynamic response and good accuracy ✓ Meet the requirements of real-time applications and dynamic estimation ✓ Closed-loop control	× Diverges if the model is not precise as it is highly dependent on the employed model × High computational load
Data-Driven Methods	✓ Provides high accuracy ✓ Handles the high non-linearity of the system with good mapping approximation ✓ Aging model is not required for system analysis	✓ Complex since extensive test data as well as massive training are required ✓ Sensitive to measurement noise

estimation methods can be categorized into direct, model-based, and data-driven [17], [18]. Table 1 compares the three methods.

Data-driven SoC estimation methods have gained much attention due to the progress witnessed in deep learning in terms of reduced cost, size, and power [19]. Deep learning methods utilize the historical data measured/ obtained from the battery based on experimental results and predict the aging patterns, estimating the SoC and SoH. In other words, the battery data sets are trained to generate a mathematical description approximating the behavior of the battery to estimate the SoC and predict the SoH [2]. Artificial neural networks (ANN) and support vector machines (SVM) are used as the main tools in deep learning methods [2]. Deep learning provides a valuable means for extracting the collected data over time for SoC estimation. It can solve the non-linearity and instability problems in the battery's data collection. Nevertheless, training can be complex and requires time before employing the algorithm since this method is based on a large amount of experimental offline data. The current, voltage, and temperature characteristics are trained to provide the SoC mapping model [19], [22].

Several research studies have been introduced for Li-ion batteries SoC estimation using machine learning [19], [23]-[33]. In [19], an SoC balancing method is presented considering the SoH of the battery cells. SoC estimator, which is ANN-based, is developed to predict the battery cells' available capacity. The presented mechanism in [19] draws energy at a lower rate for low SoH battery cells and at a higher rate for high SoH battery cells such that all the battery cells reach the end of the discharge process simultaneously. In [29], a machine learning method is proposed for SoC estimation for Li-ion batteries. The proposed method utilizes dynamic nonlinear auto-regressive models with exogenous input neural network (NARX) with long short-term memories (LSTM) to improve the accuracy estimation. This hybrid combination enhanced the root mean square error by approximately 60% compared to the standard LSTM. In [30], a deep neural network (DNN) approach is presented for the SoC estimation of Li-ion batteries in EVs. The presented approach in [30] is developed by varying the number of hidden layers. It is found that increasing the number of hidden layers reaching four layers reduces the error rate and improves the SoC estimation. In [32]-[34], SoH estimation methods have been employed for Li-ion batteries using support vector regression (SVR), Gaussian process regression, and neural networks, respectively. Data-driven methods demonstrate SoC estimation with high accuracy but at the expense of massive data set requirements.

The model-based method utilizes the electrochemical or electrical equivalent circuit models discussed earlier [21]. Model-based SoC estimation approaches can be classified into stochastic estimation and non-linear observers, categorized as physical model methods. The stochastic estimation includes several Kalman filter (KF) techniques, including extended Kalman filter (EKF), iterated EKF, and sigma-point KF [2]. The KF method provides accurate estimation and system robustness. However, building an accurate battery model is challenging due to the variations in the internal resistance and capacitance. Stochastic estimation also includes the particle filtering (PF) technique, which handles severe non-linearities and non-Gaussian noise. Stochastic estimation, including KFs and PFs, is considered a favored choice in practice since it can be applied to almost every battery model to suppress the noise affecting the overall battery system. However, KFs and PFs are competitive since more computational resources are required, especially for low-dimensional battery models. The non-linear SoC observers have also gained attention in the past several years. It covers several techniques, including Luenberger observer, sliding mode observer, adaptive observer, robust observer, back-stepping observer, and output-injection observer. Although KFs require more computational resources, such algorithms are most favored by researchers due to their prominent features in suppressing noise [35].

EKF is considered the most appropriate algorithm for SoC

estimation, in which the non-linear functions are linearized through partial derivative and Taylor series expansion. The accuracy of this algorithm depends on how accurately the battery model parameters are identified and the pre-knowledge of the noise variable. In which incorrect noise variable causes divergence. To avoid divergence and improve stability, this issue is solved through the AEKF by incorporating a moving window method with the EKF to update the covariance matrices. Nonetheless, the moving window adds an extra computational burden. This is solved using a forgetting factor-based AEKF, which provides more variations throughout the estimation process considering the recent data samples. Nevertheless, the accuracy of the SoC estimation is not guaranteed due to the battery modeling offline indentation. The dual Kalman filter (DKF) solves this problem, simultaneously updating the battery model parameters [35].

In [35], a dual forgetting factor adaptive extended Kalman filter (DFF-AEKF) is proposed for SoC and SoE estimation. The presented method in [35] provides high accuracy and strong robustness. The estimation method in [22] presents less sensitivity to the initial error condition and converges to the actual values faster than the AEKF algorithm. In [36], an AEKF is combined with adaptive recursive least squares (RLS) for SoC estimation of Li-ion batteries. The presented method offers online tracking for the model parameters and system noise. In [37], an adaptive forgetting factor recursive least square algorithm is introduced for identifying the battery model parameters. In [38], an adaptive algorithm is added to the unscented Kalman filter (UKF) to realize adaptive noise updates. However, the robustness of the algorithm is not improved. In [39], a dual UKF is proposed to achieve fast convergence and stable performance despite a large initial estimation error. However, the filtering process does not realize adaptive noise updates. In [40], singular value decompositions are used along with the UKF to deal with the non-positive error covariance matrix. This is done to ensure stability and realize adaptive noise updates. However, the singular value decomposition cannot guarantee the accuracy of the covariance matrix. In [41], a fading factor-based UKF is introduced for Li-ion battery SoC estimation. In [42], the partial adaptive forgetting factor least square method is presented for SoC estimation during deep discharging. To the author's knowledge, the adaptive forgetting factor concept is either applied to the noise covariance matrices or the states covariance matrix. In this regard, this paper studies the effect of employing three forgetting factors in the AEKF algorithm to consider high measurement noise levels while maintaining a simple structure to consider the environmental and vibrational circumstances encountered by the operation of EBs.

To improve SoC estimation accuracy, several studies have introduced hybrid solutions, combining different estimation methods [43]-[45]. The main aim of hybrid methods is to combine the advantages of the methods presented in Table 1.

Although several research studies have been proposed in literature for SoC estimation methods [2], [6]-[50], these methods are insufficient in achieving the best filtering performance, considering the high measurement noise level and environmental circumstances encountered during the EB operation, especially considering the expected higher noise levels in EBs. Therefore, different and random noise levels should be considered to examine the applicability of the SoC estimation algorithms for EB applications. In addition, most of the introduced algorithms focus on employing a forgetting factor component for the noise covariance matrices without considering the effect of the states covariance matrix on the gain of the KF. To clarify, the Kalman gain is affected by the change in the states covariance matrix, which would affect the accuracy of the estimation technique. Moreover, battery parameters are influenced by several factors, including ambient temperature, SoC, charging current, and aging factors. Among these factors, the ambient temperature highly affects the battery parameters. Therefore, the effect of the ambient temperature on the battery parameters should be investigated. In this regard, the main contribution of this paper is to introduce the temperature-dependent Triple Forgetting Factor Adaptive Extended Kalman Filter (TFF-AEKF) for SoC estimation to provide better SoC estimation accuracy and faster convergence with the existence of high measurement noise level considering system complexity and computational efforts. To further illustrate, three forgetting factors are employed in the Adaptive Extended Kalman Filter (AEKF) algorithm. The first forgetting factor (FF) is applied to the state's covariance matrix to neutralize the problem mentioned earlier, while the second and third FFs are applied to the process and measurement noise covariance matrices. The proposed TFF-AEKF is evaluated using Matlab/ Simulink software using the second-order RC equivalent model. In addition, the relationship between the battery's internal resistance and the open circuit voltage with the ambient temperature is studied. Moreover, the proposed algorithm is compared to the conventional AEKF and the Dual FFAEKF (DFF-AEKF). Four performance indicators are used to validate the effectiveness of the TFF-AEKF, which are Maximum Absolute Error (MaxAE), Mean Absolute Error (MAE), Root Mean Square Error (RMSE), and convergence time. It is concluded that the presented method offers lower MaxAE, lower MAPE, lower RMSE, and faster convergence to its true value at high measurement noise level.

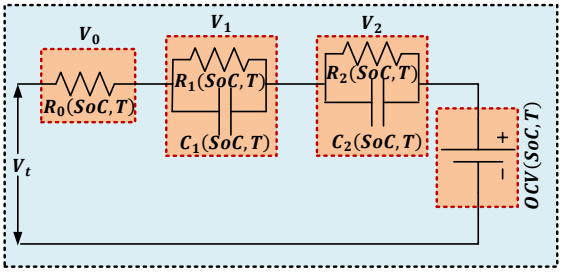

Fig. 3. Temperature dependent second order RC model of a Li-ion battery [37], [46]-[48].

This paper is structured as follows: Section 2 reviews the SoC estimation methods introduced in the literature, Section 3 presents the second-order battery model, Section 4 presents the TFF-AEKF algorithm, and Section 5 presents the Matlab/

Simulink results. Finally, Section 6 summarizes the key outcomes of this work.

2. Li-Ion Battery Modeling

Since the equivalent circuit model of the Li-ion battery is less complex, it is usually utilized for the SoC estimation in model-based methods [35]. The second-order RC model of the Li-ion battery shown in Fig. 3 involves a series of internal resistance (R_0), a resistor and capacitor branches with a parallel connection $(R_1C_1)\&(R_2C_2)$, and a voltage source equivalent to the battery cell open circuit voltage (OCV)[37], [46]-[48]. In which, R_1 and R_2 represent the dynamic resistances, $C_1$and C_2 represent the dynamic capacitances, and V_t is the terminal voltage of the battery.

The state-space equation of the battery can be obtained from Fig. 3 and can be expressed as follows:

$$\begin{cases} \dot{V}_1 = -\dfrac{1}{C_1(SoC,T)}\left(\dfrac{V_1}{R_1(SoC,T)} + I\right) \\ \dot{V}_2 = -\dfrac{1}{C_2(SoC,T)}\left(\dfrac{V_2}{R_2(SoC,T)} + I\right) \\ V_t = OCV(SoC,T) - V_1 - V_2 - IR_0(SoC,T) \end{cases} \tag{1}$$

The SoC of the battery represents the remaining charges stored in the battery, and it can be expressed as follows:

$$SoC_{k+1} = SoC_k - \frac{\eta_c I_k T_s}{C_A} \tag{2}$$

Where, η_c is the charging and discharging efficiency, $I_k$is the current of the battery at k. In which, k is the k^{th}sample time, C_A is the actual capacity and T_s is the sampling time.

3. Triple Forgetting Factor Adaptive Extended Kalman Filter (TFF-AEKF)

In this section, the proposed TFF-AEKF algorithm is presented. A typical representation of a non-linear system using discrete-time state space equations is expressed as follows:

$$\begin{cases} X_k = A_{k-1}X_{k-1} + B_{k-1}u_{k-1} + \omega_{k-1} \\ Y_k = C_kX_k + D_ku_k + \upsilon_k \\ \omega_k \approx N(0, P_{\omega,k}) \\ \upsilon_k \approx N(0, P_{v,k}) \end{cases} \tag{3}$$

Where, X_k is the system's state, Y_k is the system's output vector, ω_k and υ_k are the zero mean small white noise signals with the covariance matrices $P_{\omega,k}$, and $P_{v,k}$, respectively and u_k is the control variable matrix. A_k, B_k, $C_k$and D_k are matrices that depend on the system dynamics, and k denotes the system vector time step.

To avoid divergence resulting from the AEKF estimation method employed in non-linear systems, the AEKF is modified to employ three forgetting factors. One forgetting factor is applied to the states' covariance matrix, and two forgetting factors are applied to update the process and measurement noise covariance matrices.

The TFF-AEKF steps can be summarized as follows:

- Initialization: the mean and the covariance are initialized at step $k = 0$

$$\begin{cases} \hat{x}_0^+ = E(x_0) \\ P_{x,0}^+ = E[(x_0 - \hat{x}_0^+)(x_0 - \hat{x}_0^+)^T] \end{cases} \tag{4}$$

Where, $\hat{x}_0^+$ and $P_{x,0}^+$ represents the estimated initial state and covariance matrix error, respectively. The superscript denotes the posterior values $(+)$, the estimated value is defined by the circumflex $(\wedge)$, the predicted value is represented by the tilde $(\sim)$, and the matrix transportation is indicated by (T).

- Prediction: The prior state and its covariance matrix are obtained from the projection of step $k-1$ to step k. The predicted state estimation and priori covariance matrix can be expressed in (6) and (7), respectively:

$$\hat{x}_k^- = \hat{A}_{k-1}\,\hat{x}_{k-1}^+ + \hat{B}_{k-1}\,u_{k-1} \tag{5}$$

$$P_{x,k}^- = \hat{A}_{k-1}P_{x,k-1}^+\hat{A}_{k-1}^T + P_{\omega,k-1} \tag{6}$$

Where, $\hat{A}_k = \left.\frac{\partial F(x_k,\theta_k,I_k)}{\partial x_k}\right|_{x_k=\hat{x}_k^-}$, $\hat{B}_{k-1} = \left.\frac{\partial F(x_k,\theta_k,I_k)}{\partial \omega_k}\right|_{\omega_k=\hat{\omega}_k^-}$, and $P_{\omega,k}$ is the covariance matrix of the process.

- Correction: In this stage, the difference between the actual and predicted measurements is calculated from the prior estimation and utilized to obtain an enhanced posterior estimation. The Kalman gain matrix, posteriori state estimation, and posteriori covariance matrix can be expressed as in (7), (8), and (9), respectively:

$$L_k = P_{x,k}^-\hat{C}_k^{xT}\left[\hat{C}_k^x P_{x,'k}^-\hat{C}_k^{xT} + D_k^x P_{v,k}^- D_k^{xT} + a_{1,k}\right]^{-1} \tag{7}$$

$$\hat{x}_k^+ = \hat{x}_k^- + L_k[y_k - \hat{y}_k] \tag{8}$$

$$P_{x,k}^+ = \frac{1}{a_{1,k}}\left[P_{x,k}^- - L_kP_{y,k}^-L_k^T\right] \tag{9}$$

Where, $\hat{C}_k^x = \left.\frac{\partial F(x_k,\theta_k,I_k)}{\partial x_k}\right|_{x_k=\hat{x}_k^+}$, $D_k^x = \left.\frac{\partial F(x_k,\theta_k,I_k)}{\partial v_k}\right|_{v_k=\hat{v}_k^-}$, $P_{v,k}$ is the covariance of the noise v_k, and $a_{1,k}$ is a variable forgetting factor applied to the state covariance matrix in the correction stage and defined as follows:

$$a_{1,k} = a_{1,min} + (1 - a_{1,min})h^{\varepsilon_k} \tag{10}$$

$$\varepsilon_k = round\left(\left(\frac{e_k}{e_{base}}\right)^2\right) \tag{11}$$

Where, $a_{1,min}$ is the forgetting factor's lowest value, and according to [37], the range of the forgetting factor is between 0.95 to 1, and the practical data are more accurate when the

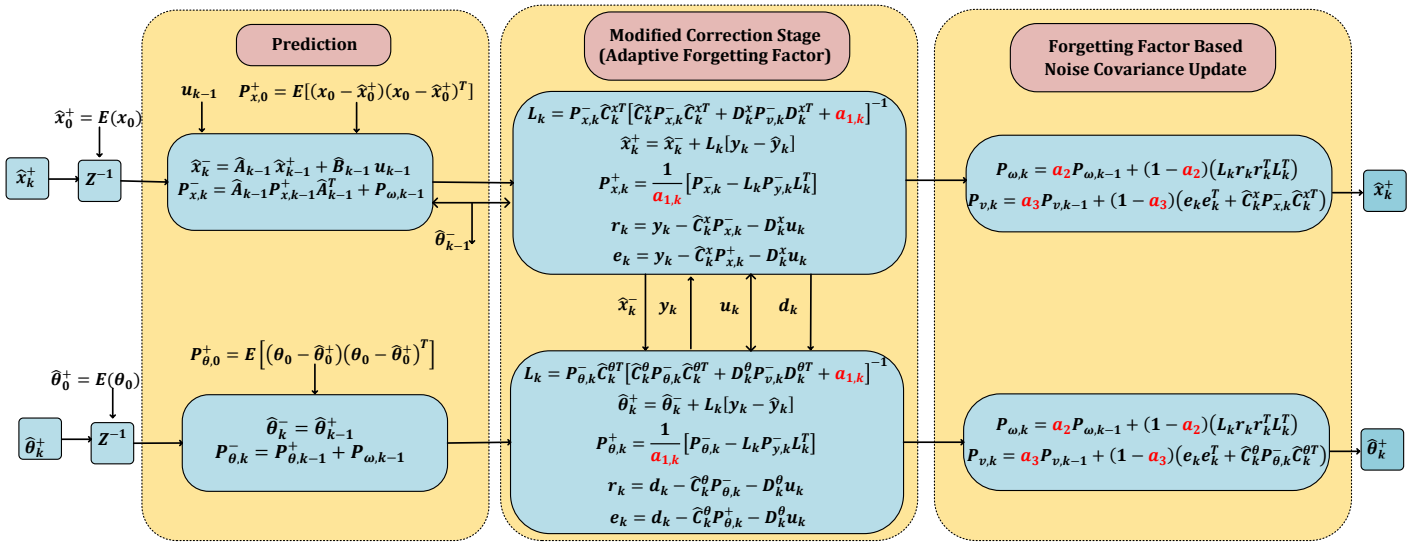

Fig. 4. TFF-AEKF Algorithm.

range is between 0.98 to 1. Consequently, in this work, $a_{1,min}$ is selected to be 0.98. This forgetting factor is added to neutralize the effect of the state covariance matrix on the gain of the KF algorithm. h is the sensitivity factor and is chosen as any value from 0 to 1. This factor indicates how sensitive is the forgetting factor to the errors:

- When h is near 1, a slow response is resulted since the forgetting factor moves slowly from 1 to 0.98.
- When h is near 0, a fast response is obtained since the forgetting factor moves quickly from 1 to 0.98. Choosing the sensitivity factor close to 0 is not recommended since this will lead to a swift response, reducing accuracy.

As a result, h is selected as 0.9 considering the tradeoff between the fast response and accuracy.

The term e_k in (11) represents the error at time k and e_{base} is the reference error. As seen from (11), the forgetting factor $a_{1,k}$ decreases when e_k is greater than e_{base}. When the estimated SoC error is less than e_{base}, the forgetting factor $a_{1,k}$ converges to a larger value, and when the estimated SoC error is greater than e_{base}, the forgetting factor $a_{1,k}$ converges to a smaller value. It can be observed from (11) that as the error increases, the forgetting factor reduces, which varies according to the SoC estimation error.

In the TFF-AEKF, the process noise covariance matrix and the measurement noise covariance matrix are updated as expressed in (12) and (13), respectively, by applying more weight on the current values through the forgetting factor a which can vary from 0 to 1. The concept of the forgetting factor is to put more weightage on the previous values in the update stage of the noise covariance matrices. This is done to provide less fluctuation and longer time delays to detect the changes. In this regard, the values of a_2 and a_3 are selected to be greater than 0.9.

$$P_{\omega,k} = a_2 P_{\omega,k-1} + (1-a_2)(L_k r_k r_k^T L_k^T) \tag{12}$$

$$P_{v,k} = a_3 P_{v,k-1} + (1-a_3)\left(e_k e_k^T + \hat{C}_k^x P_{x,k}^- \hat{C}_k^{xT}\right) \tag{13}$$

Where, $r_k = y_k - \hat{C}_k^x P_{x,k}^- - D_k^x u_k$ denoted as the innovation measurement and $e_k = y_k - \hat{C}_k^x P_{x,k}^+ - D_k^x u_k$ denoted as the residual.

In this work, the three covariance matrices, including the states, process noise, and observation noise covariance matrices, are updated to obtain better accuracy by adopting three forgetting factors to introduce adaptive estimation. The forgetting factor improves the estimation accuracy and increases the system convergence compared to the conventional AEKF and the DFF-AEKF.

The TFF-AEKF algorithm is presented in Fig. 4. The presented technique is capable of updating the parameters of the battery model, SoC, and the unidentified noise covariance matrices. In which the SoC and the parameter estimation of the battery can be expressed as follows:

$$\begin{cases} X_k = [SoC_k \quad V_{1,k} \quad V_{2,k}]^T \\ x_{k+1} = F(x_k, \theta_k, I_k, T) + \omega_k^x \\ y_k = G(x_k, \theta_k, I_k, T) + v_k^x \end{cases} \tag{14}$$

Where, $F(.)$ and $G(.)$ represent the nonlinear functions of the state vector x_k, the battery model parameter θ_k, and the battery input current I_k, and the battery's temperature T.

$$F(.) = \hat{A}_k \begin{bmatrix} SoC_k \\ V_{1,k} \\ V_{2,k} \end{bmatrix} + \begin{bmatrix} \frac{-\eta_c T_s}{C_A} \\ R_1\left(1 - e^{-T_s/r_1}\right) \\ R_2\left(1 - e^{-T_s/r_2}\right) \end{bmatrix} B I_k \tag{15}$$

$$G(.) = OCV(SoC_k, T) - V_{1,k}(SoC_k, T) - V_{2,k}(SoC_k, T) - I_k R_0(SoC_k, T) \tag{16}$$

Where, T_s is the sampling time, and B is a diagonal matrix expressed as : $\begin{bmatrix} 1 & 0 & 0 \\ 0 & 1 & 0 \\ 0 & 0 & 1 \end{bmatrix}$.

The battery state Jacobian matrix can be expressed as follows:

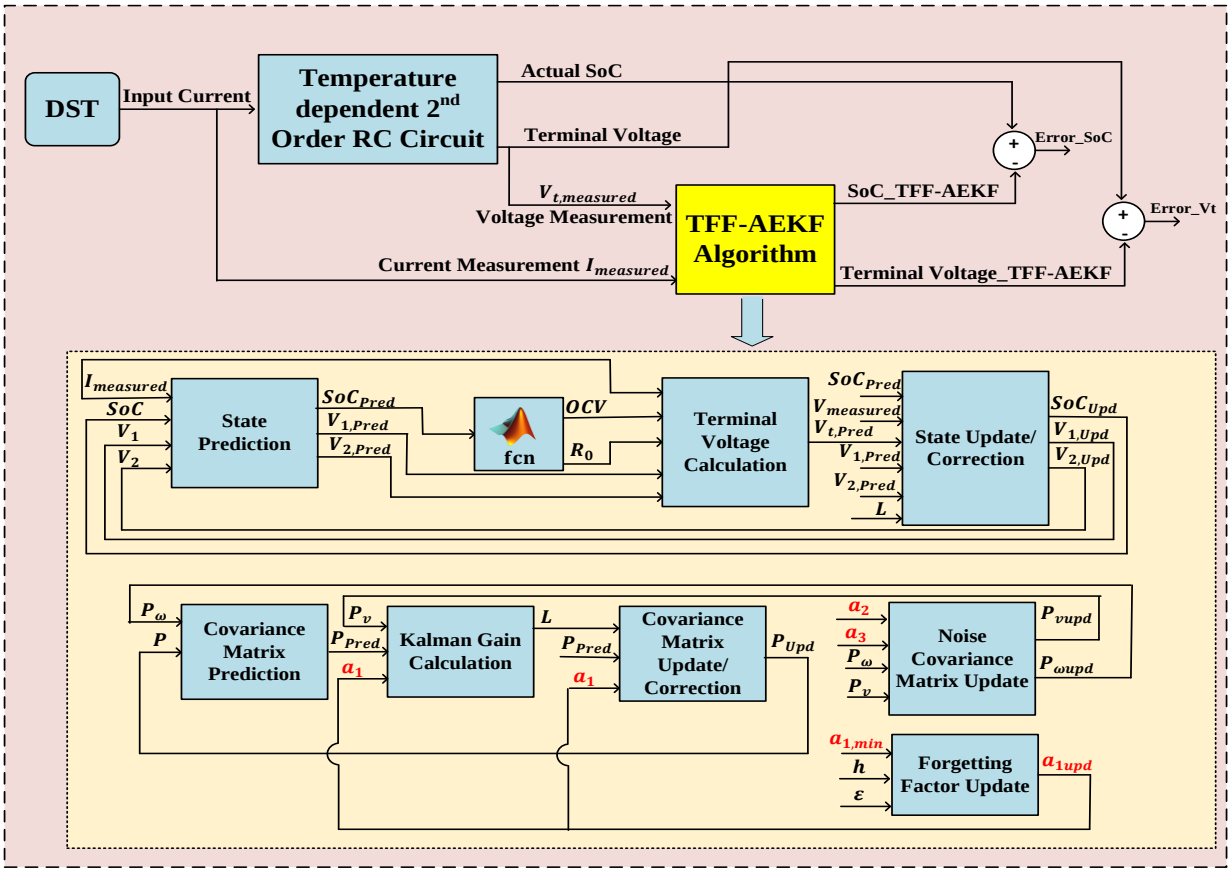

Fig. 5. TFF-AEK Simulink Block Diagram.

$$\hat{A}_k = \left.\frac{\partial F(.)}{\partial x_k}\right|_{x_k=\hat{x}_k^-} = \begin{bmatrix} 1 & 0 & 0 \\ 0 & \frac{1}{e^{-T_s/\tau_1}} & 0 \\ 0 & 0 & \frac{1}{e^{-T_s/\tau_2}} \end{bmatrix} \quad (17)$$

$$\hat{C}_k^x = \left.\frac{\partial G(.)}{\partial x_k}\right|_{x_k=\hat{x}_k^-} = \left[\frac{\partial OCV}{\partial SoC_k} - 1 - 1\right] \quad (18)$$

Where, $\tau_1 = R_1C_1$ and $\tau_2 = R_2C_2$.

4. Performance Assessment

This section defines the performance indicators used to evaluate the proposed technique. In addition, the Matlab/Simulink platform is used to evaluate the performance of the TFF-AEKF for SoC estimation. In this study, a Li-ion battery with a nominal capacity of 1.5 Ah and a rated voltage of 4.1 V is utilized.

Several types of performance evaluation are introduced to evaluate and assess the results obtained from the SoC estimation and battery modeling. In this work, the convergence time, the Maximum Absolute Error (MaxAE), the Mean Absolute Error (MAE), and the Root Mean Square Error (RMSE) are obtained to evaluate the performance of the proposed algorithm and verify its effectiveness. The MaxAE, MAE, and the RMSE can be expressed as follows:

$$MaxAE = max[(Estimated)_k - (Measured)_k] \quad (19)$$

$$MAE = \frac{1}{N}\sum_{k=1}^{N}((Estimated)_k - (Measured)_k) \quad (20)$$

$$RMSE = \sqrt{\frac{1}{N}\sum_{k=1}^{N}((Estimated)_k - (Measured)_k)^2} \quad (21)$$

Where N is the number of sample points. In this work, the battery terminal voltage and the estimated SoC are evaluated using (19), (20), and (21). The evaluation matrices compare the conventional AEKF and the DFF-AEKF with the TFF-AEKF.

The battery parameters are identified using the experimental data presented in [51] and[52]. The experimental data and curve

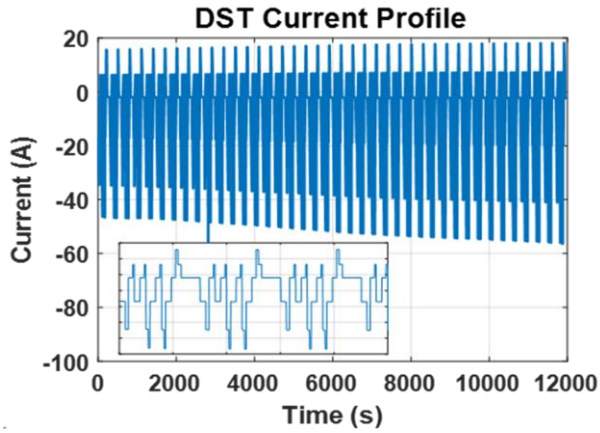

Fig. 6. Dynamic Stress Test current profile.

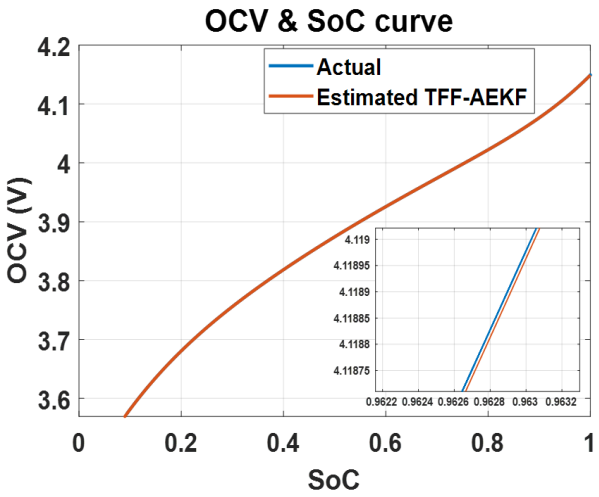

Fig. 7. OCV and SoC actual and estimated curve using TFF-AEKF algorithm.

fitting are applied to obtain the battery's parameters using mathematical equations studied in [52].

According to the conducted experiments in [35], the relationship between the battery's SoC and the OCV is represented as a polynomial fitted equation and can be expressed as follows:

$$OCV(SoC_k, T) = \sum_{i=0}^{n} k_i SoC^i, i = 1, 2, \dots, n \quad (24)$$

Where k_i is the n order polynomial coefficients determined using the robust linear least square method.

Fig. 5 presents the detailed block diagram implemented in Simulink to evaluate the performance of the TFFAEK for SoC estimation considering the three forgetting factors. A dynamic stress test (DST) is applied in Simulink for the SoC estimation, where the current profile is shown in Fig. 6. In Fig. 7, the OCV-SoC curve is presented using the polynomial fitted equation in (24).

As per the studies presented in [53]-[56], the normal operating temperature for Li-ion batteries ranges from 45℃ to 65 ℃. It is worth mentioning that there is a high possibility of going through a thermal runway when operating beyond normal operating conditions. Utilizing the battery at extremely high temperatures (starting from 100 ℃ and above) will cause battery destruction due to aging and thermal runaway. On the contrary, utilizing the battery at a low temperature (below 0℃) will cause the loss of power delivery. Operating at high temperatures leads to more power delivery since the internal resistance is minimal, which made the relationship between the internal resistance and the ambient temperature of high interest to be studied and discussed.

In this regard, the proposed concept is tested under different operating temperatures, varying from 5 ℃ to 55 ℃. Fig. 8 presents the effect of the temperature on the OCV, the internal resistance of the battery, and the end-of-life resistance. As can be observed from Fig. 8 (a), the OCV of the lithium-ion battery gradually decreases as the ambient temperature rises for the same SoC. Similarly, as shown in Fig. 8 (b) and (c), the internal resistance reduces significantly as the temperature increases. Therefore, it is preferable to utilize the employed battery at high temperatures such that it does not exceed 65 ℃ due to the low internal resistance properties. However, another problem that results from long-term use is fast battery degradation at high temperatures. In other words, utilizing the battery at a high temperature will allow for better performance to be extracted from the employed battery. Nonetheless, the battery will degrade faster and will not last for a long time, which will accordingly affect the State-of-Health (SoH) of the battery.

Results presented in Fig. 9 are obtained from the DST applied. The sampling time is set to $1\,s$ solving for 12000 steps/ seconds. As shown in Figs 9 (a) and (d), the TFF-AEKF estimated SoC and terminal voltage track the reference value with an error of 0.01 for the estimated SoC and $0.1\,V$ for the estimated terminal voltage. Figures 9 (b) and (e) present the estimation error for the SoC and terminal voltage, respectively. As shown from Fig. 9 (c) and Fig. 9 (f), the TFF-AEKF converges to the actual value at $20\,s$ for the SoC and converges at $15\,s$ for the terminal voltage.

To compare the proposed TFF-AEKF with the conventional AEKF and the DFF-AEKD, a change is introduced to the measurement noise level at $6000\,s$. Fig. 10 presents the Gaussian noise introduced to the DST current profile. To

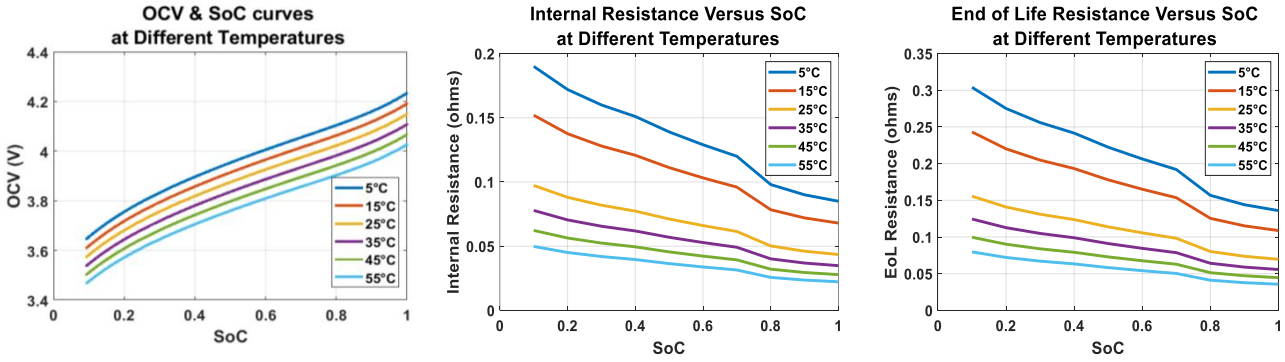

(a) (b) (c)

Fig. 8: Effect of the temperature on the OCV and the battery's internal resistance; (a) Relation between the OCV and ambient temperature, (b) Relation between the internal resistance and ambient temperature, (c) Relation between End of Life resistance and ambient temperature.

This article has been accepted for publication in IEEE Transactions on Transportation Electrification. This is the author's version which has not been fully edited and content may change prior to final publication. Citation information: DOI 10.1109/TTE.2024.3514704

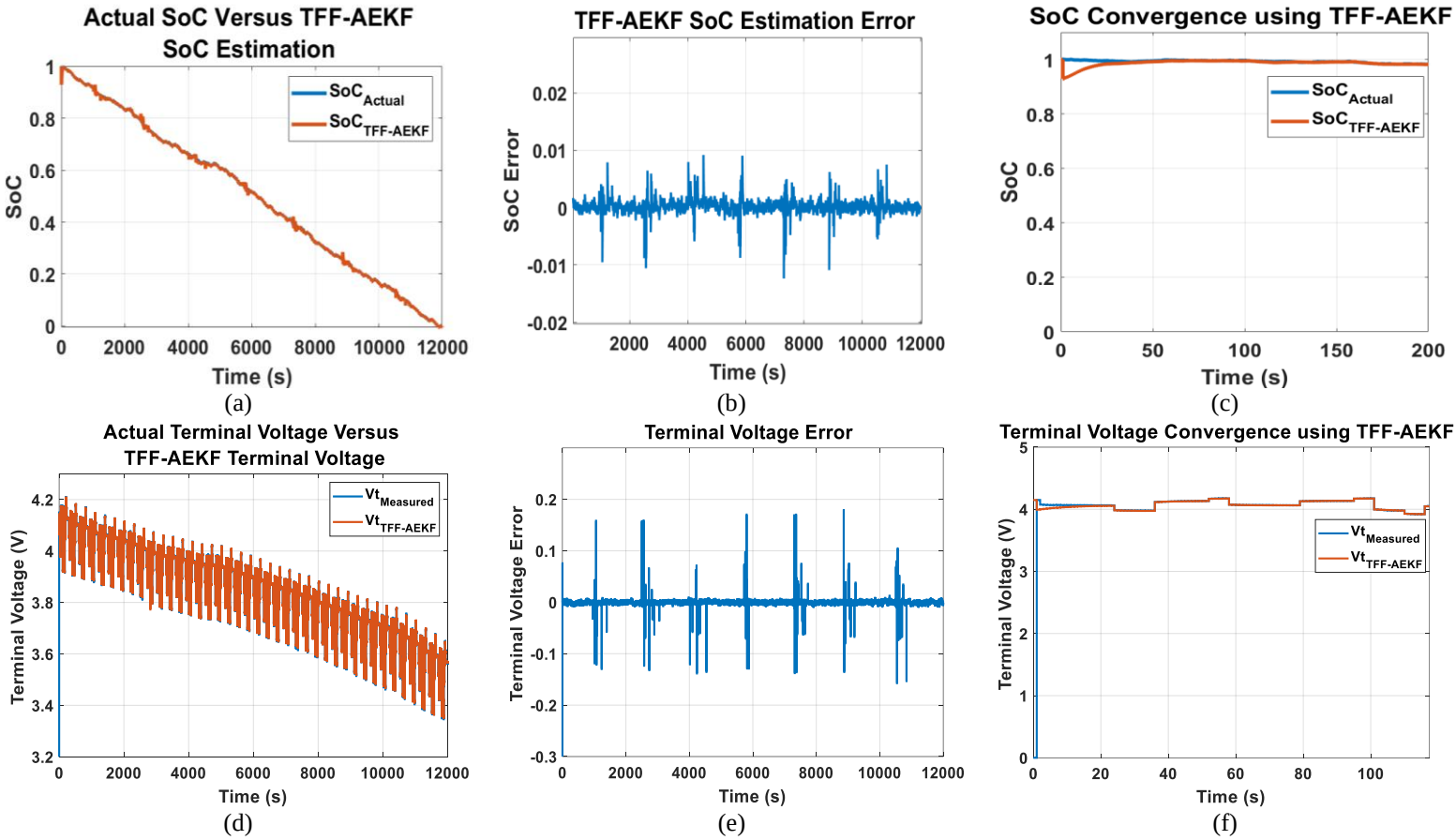

Fig. 9. Simulation Results under DST; (a) Actual SoC versus TFF-AEKF SoC estimation; (b) SoC Error; (c) Convergence time; (d) Measured terminal voltage versus TFF-AEKF terminal voltage; (e) Terminal voltage error; (f) Convergence time.

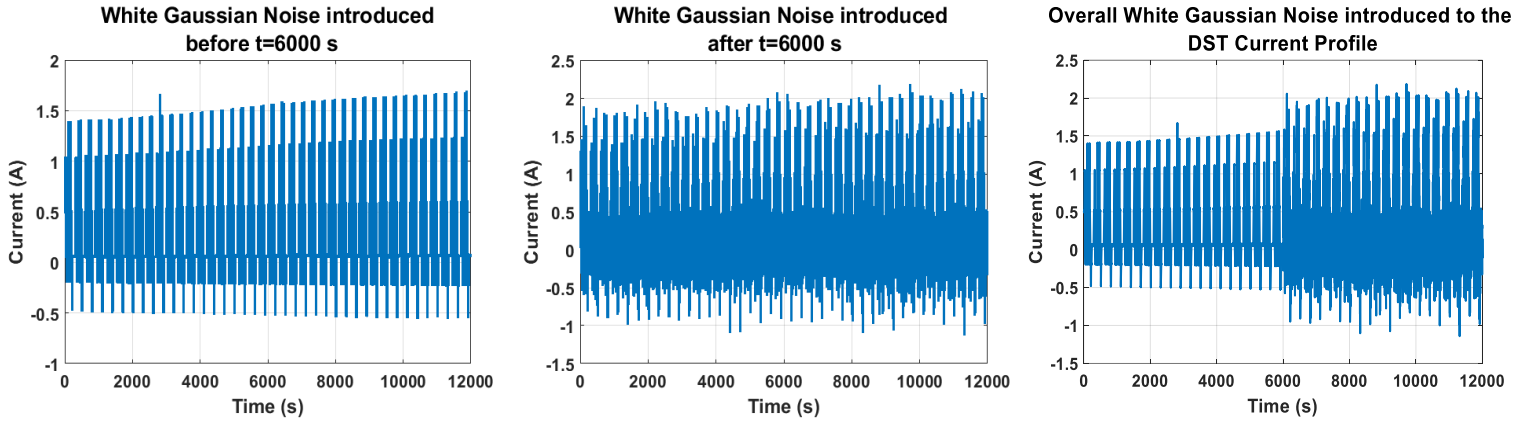

Fig. 10. White Gaussian noise introduced to the applied current profile; (a) before $t = 6000\ s$, (b) after $t = 6000\ s$, (c) Noise for the whole simulation time.

illustrate, Fig. 10 (a) presents the noise before $t = 6000\ s$, Fig. 10 (b) presents the noise added after $t = 6000\ s$, and Fig. 10 (c) presents the overall noise for the whole simulation time.

As seen from Fig. 11 (a), when high measurement noise is considered, the SoC estimation using the TFF-AEKF converges faster to the reference value when compared to the AEKF and the DFF-AEKF. In addition, the performance of the conventional AEKF presents high steady-state error when a high noise level is introduced. The DFF-AEKF converges to the reference SoC and terminal voltage after $4000\ s$ while the proposed algorithm converges after $500\ s$ from the change. Therefore, it can be said that the TFF-AEKF provides better accuracy and fast convergence speed. Similar behavior can also be observed from the terminal voltage results in Fig. 11 (b).

Fig. 11 presents a zoomed-in illustration of all the results, Which shows the effectiveness of the TFF-AEKF in terms of accuracy and convergence compared to the conventional AEKF and the DFF-AEKF.

It is worth mentioning that the other Kalman filter approaches, such as Unscented KF, Cubature KF, and Iterated KF, are not considered in the comparison since such approaches involve a heavy computational burden, which would add more complexity to the system [57]. Computational complexity is considered an important factor when it comes to hardware

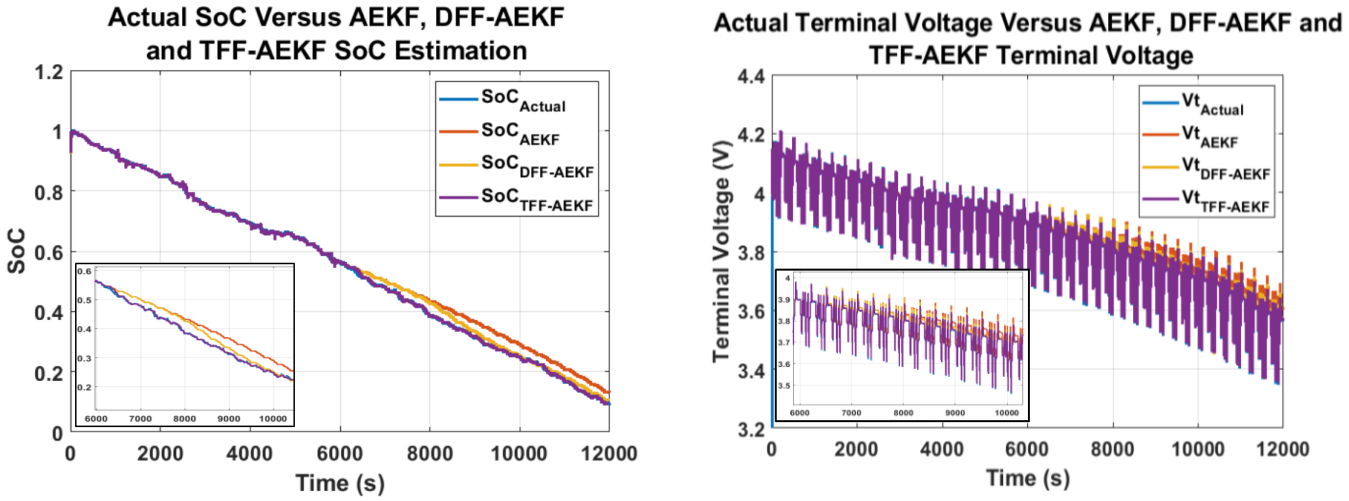

(a) (b)

Fig. 11. Simulation Results with high measurement noise considered at 6000 s; (a) SoC estimation using AEKF, DFF-AEKF, and TFF-AEKF, (b) Terminal voltage using AEKF, DFF-AEKF, and TFF-AEKF.

Table 2. Performance indicators for the AEKF, DFF-AEKF, and TFF-AEKF under DST.

Parameter		AEKF	DFF-AEKF	TFF-AEKF
V_t	$MaxAE$	0.185 V	0.161 V	0.157 V
	MAE	0.0012 V	0.0005 V	0.00004 V
	$RMSE$	0.0067 V	0.0037 V	0.0024 V
	Convergence Time	$> 6000\ s$	4000 s	$\leq 5\ s$
SoC	$MaxAE$	0.059	0.045	0.017
	MAE	0.0185	0.0083	0.0001
	$RMSE$	0.028	0.015	0.0028
	Convergence Time	$> 6000\ s$	4000 s	500 s

implementation. Therefore, the applied algorithm should be implementable on a microcontroller with less complexity. In this regard, KFs that are sigma-point based are not considered in the comparison since $2N + 1$ points are used to calculate the prior mean in the time update, which increases the computational complexity, where N is the dimension of the state On the other hand, AEKFs require only one calculation/ point regardless the dimension of the state [57].

Table 2 presents the MaxAE, MAE, RMSE, and the convergence time obtained for the battery's terminal voltage and SoC under the DST for the three filters. As can be seen from Table 2, the proposed TFF-AEKF provides the lowest MaxAE, MAE, and RMSE. The proposed TFF-AEKF provides an RMSE of 0.3%, an MAE of 0.01%, and a MaxAE of 1.7% for SoC estimation. For the terminal voltage, the TFF-AEKF provides an RMSE of 2.4 mV, an MAE of 0.04 mV, and a MaxAE of 157 mV. In addition, the TFF-AEKF provides faster convergence, and this can be noticed in Fig. 11. It can be noticed that the terminal voltage and the estimated SoC using the TFF-AEKF are tracking the reference with higher accuracy when compared to the results obtained using the conventional AEKF and the DFF-AEKF. However, due to the three forgetting factors required to adaptively update the state covariance matrix and update the process and measurement noise covariance matrices, the TFF-AEKF requires more computational load/ cost.

5. Conclusion

Reliable and safe operation for the BESS is highly required. Accurate battery SoC estimation is essential in monitoring and controlling the BESS stability. Many research efforts have been made to estimate the BESS SoC and improve the estimation accuracy. However, the proposed SoC estimation methods are insufficient in achieving the best filtering performance, considering the high measurement noise level and environmental circumstances encountered during the EB operation. Therefore, this paper introduces the TFF-AEKF for SoC estimation to provide better SoC estimation accuracy and faster convergence with high measurement noise levels, considering system complexity and computational efforts. Three forgetting factors are adopted in the AEKF algorithm. The first FF is applied to the state's covariance matrix, while the second and third FFs are applied to the process and measurement noise covariance matrices, respectively. The performance of the proposed TFF-AEKF is evaluated and compared to the AEKF and the DFF-AEKF using the Matlab/ Simulink platform. It has been validated that the proposed algorithm can provide faster convergence at high measurement noise levels. In addition, results have demonstrated that the TFF-AEKF provides the lowest MaxAE, MAE, and RMSE and faster convergence to the true/ reference value. As per the results presented, the TFF-AEKF provides an RMSE of 0.3%, an MAE of 0.01%, and a MaxAE of 1.7% for SoC estimation. For the terminal voltage, the TFF-AEKF provides an RMSE of 8 mV, an MAE of 0.3mV, and a MaxAE of 140 mV. Adopting three forgetting factors improves the estimation accuracy and increases the system convergence when compared to the conventional AEKF and the DFF-AEKF, yet additional computational load is required.

ACKNOWLEDGMENT

This publication was made possible by GSRA grant GSRA9-L-1-0514-22014G from the Qatar National Research Fund (a member of Qatar Foundation) and the funding support received from Qatar National Library (QNL) for this publication. The statements made herein are solely the responsibility of the authors.

REFERENCES

[1] Q. Sun, H. Lv, S. Wang, S. Gao, and K. Wei, "Optimized State of Charge Estimation of Lithium-Ion Battery in SMES/Battery Hybrid Energy Storage System for Electric Vehicles," in *IEEE Transactions on Applied Superconductivity*, vol. 31, no. 8, pp. 1-6, Nov. 2021, Art no. 5700606.

[2] Y. Wang, H. Fang, L. Zhou, and T. Wada, "Revisiting the State-of-Charge Estimation for Lithium-Ion Batteries: A Methodical Investigation of the Extended Kalman Filter Approach," in *IEEE Control Systems Magazine*, vol. 37, no. 4, pp. 73-96, Aug. 2017.

[3] W. Zhou, Y. Zheng, Z. Pan, and Q. Lu, "Review on the Battery Model and SOC Estimation Method," *Processes*, vol. 9, no. 9, p. 1685, Sep.

[4] X. Hua, A. Thomas, and K. Shultis, "Recent progress in Battery Electric Vehicle Noise, vibration, and harshness," *Science Progress*, vol. 104, no. 1, Jan. 2021.

[5] K. Horváth and A. Zelei, "Simulating noise, vibration, and harshness advances in electric vehicle powertrains: Strategies and challenges," *World Electric Vehicle Journal*, vol. 15, no. 8, p. 367, Aug. 2024.

[6] Z. Du, L. Zuo, J. Li, Y. Liu, and H. T. Shen, "Data-Driven Estimation of Remaining Useful Lifetime and State of Charge for Lithium-Ion Battery," in *IEEE Transactions on Transportation Electrification*, vol. 8, no. 1, pp. 356-367, March 2022.

[7] J. Li *et al.*, "Parameter identification of lithium-ion batteries model to predict discharge behaviors using heuristic algorithm," *Journal of The Electrochemical Society*, vol. 163, no. 8, 2016.

[8] K. Xin, S. Wei, and C. Hongtao, "Parameter identification based on simplified electrochemical model of lithium ion battery," *Energy Storage Science and Technology*, vol. 9, no. 3, pp. 969–978, May 2020.

[9] H. Deng, L. Yang, and Z. W. Wang, "Parameter identification and SOC estimation of lithium-ion battery based on electrochemical mechanism model," *Journal of University of Shanghai for Science and Technology*, vol. 40, pp. 557–565, 2018.

[10] X. Liu, W. Li, and A. Zhou, "PNGV Equivalent Circuit Model and SOC Estimation Algorithm for Lithium Battery Pack Adopted in AGV Vehicle," in *IEEE Access*.

[11] J. Schmitt, I. Horstkötter, and B. Bäker, "Electrical lithium-ion battery models based on recurrent neural networks: A holistic approach," *Journal of Energy Storage*, vol. 58, p. 106461, Feb. 2023.

[12] W. Junping, C. Quanshi, and C. Binggang, "Support Vector Machine based battery model for electric vehicles," *Energy Conversion and Management*, vol. 47, no. 7–8, pp. 858–864, May 2006.

[13] T. Al Rafei, N. Yousfi Steiner, and D. Chrenko, "Genetic algorithm and Taguchi Method: An approach for better Li-ion cell model parameter identification," *Batteries*, vol. 9, no. 2, p. 72, Jan. 2023.

[14] Y. Yang et al., "Extreme learning machine–radial basis function neural network–based state-of-charge estimation of lithium-ion batteries assisted with fiber Bragg grating sensor measurements," *Transactions of the Institute of Measurement and Control*, Jan. 2023.

[15] Q. Wang, M. Ye, and M. Wei, "Small Dataset-Based Closed-Loop State of Charge Estimation for Pure Electric Construction Machinery With Large Sensor Error: A Case Study of 5-ton Loader," in *IEEE Transactions on Transportation Electrification*, vol. 9, no. 2, pp. 3350-3359, June 2023.

[16] A. Bavand, S. A. Khajehoddin, M. Ardakani, and A. Tabesh, "Online Estimations of Li-Ion Battery SOC and SOH Applicable to Partial Charge/Discharge," in *IEEE Transactions on Transportation Electrification*, vol. 8, no. 3, pp. 3673-3685, Sept. 2022.

[17] X. Bian, Z. Wei, J. He, F. Yan, and L. Liu, "A Two-Step Parameter Optimization Method for Low-Order Model-Based State-of-Charge Estimation," in *IEEE Transactions on Transportation Electrification*, vol. 7, no. 2, pp. 399-409, June 2021.

[18] M. Shehab El Din, A. A. Hussein, and M. F. Abdel-Hafez, "Improved Battery SOC Estimation Accuracy Using a Modified UKF With an Adaptive Cell Model Under Real EV Operating Conditions," in *IEEE Transactions on Transportation Electrification*, vol. 4, no. 2, pp. 408-417, June 2018.

[19] Z. Xia and J. A. Abu Qahouq, "State-of-Charge Balancing of Lithium-Ion Batteries With State-of-Health Awareness Capability," in *IEEE Transactions on Industry Applications*, vol. 57, no. 1, pp. 673-684, Jan.-Feb. 2021.

[20] D. N. T. How, M. A. Hannan, M. S. H. Lipu, and P. J. Ker "State of charge estimation for lithium-ion batteries using model-based and data-driven methods: A review," *IEEE Access*, vol. 7, pp. 136116–136136, 2019.

[21] F. Naseri, E. Schaltz, D. -I. Stroe, A. Gismero and E. Farjah, "An Enhanced Equivalent Circuit Model With Real-Time Parameter Identification for Battery State-of-Charge Estimation," in *IEEE Transactions on Industrial Electronics*, vol. 69, no. 4, pp. 3743-3751, April 2022.

[22] M. S. H. Lipu, M. A. Hannan, A. Hussain, M. H. M. Saad, A. Ayob, and M. Uddin, "Extreme learning machine model for state of charge estimation of lithium-ion battery using gravitational search algorithm," *IEEE Trans. Ind. Appl*., vol. 55, no. 4, pp. 4225–4234, Jul./Aug. 2019.

[23] F. Yang, X. Song, F. Xu, and K.-L. Tsui, "State-of-charge estimation of lithium-ion batteries via long short-term memory network," *IEEE Access*, vol. 7, pp. 53792–53799, 2019.

[24] Z. Huang, F. Yang, F. Xu, X. Song, and K. Tsui, "Convolutional gated recurrent unit–recurrent neural network for state-of-charge estimation of lithium-ion batteries," *IEEE Access*, vol. 7, pp. 93139–93149, 2019.

[25] E. Chemali, P. J. Kollmeyer, M. Preindl, R. Ahmed and A. Emadi, "Long Short-Term Memory Networks for Accurate State-of-Charge Estimation of Li-ion Batteries," in *IEEE Transactions on Industrial Electronics*, vol. 65, no. 8, pp. 6730-6739, Aug. 2018.

[26] A. A. Hussein, "Adaptive Artificial Neural Network-Based Models for Instantaneous Power Estimation Enhancement in Electric Vehicles' Li-Ion Batteries," in *IEEE Transactions on Industry Applications*, vol. 55, no. 1, pp. 840-849, Jan.-Feb. 2019.

[27] M. A. Hannan *et al*., "SOC Estimation of Li-ion Batteries With Learning Rate-Optimized Deep Fully Convolutional Network," in *IEEE Transactions on Power Electronics*, vol. 36, no. 7, pp. 7349-7353, July 2021.

[28] C. She, Y. Li, C. Zou, T. Wik, Z. Wang, and F. Sun, "Offline and Online Blended Machine Learning for Lithium-Ion Battery Health State Estimation," in *IEEE Transactions on Transportation Electrification*, vol. 8, no. 2, pp. 1604-1618, June 2022.

[29] M. Wei, M. Ye, J. B. Li, Q. Wang, and X. Xu, "State of Charge Estimation of Lithium-Ion Batteries Using LSTM and NARX Neural Networks," in *IEEE Access*, vol. 8, pp. 189236-189245, 2020.

[30] D. N. T. How, M. A. Hannan, M. S. H. Lipu, K. S. M. Sahari, P. J. Ker, and K. M. Muttaqi, "State-of-Charge Estimation of Li-Ion Battery in Electric Vehicles: A Deep Neural Network Approach," in *IEEE Transactions on Industry Applications*, vol. 56, no. 5, pp. 5565-5574, Sept.-Oct. 2020.

[31] L. Zhang, K. Li, D. Du, Y. Guo, M. Fei, and Z. Yang, "A Sparse Learning Machine for Real-Time SOC Estimation of Li-ion Batteries," in *IEEE Access*, vol. 8, pp. 156165-156176, 2020.

[32] Y. Guo, K. Huang, and X. Hu, "A state-of-health estimation method of lithium-ion batteries based on multi-feature extracted from constant current charging curve," *J. Energy Storage*, vol. 36, Apr. 2021.

[33] K. Liu, Y. Shang, Q. Ouyang, and W. D. Widanage, "A data-driven approach with uncertainty quantification for predicting future capacities and remaining useful life of lithium-ion battery," *IEEE Trans. Ind. Electron*., vol. 68, no. 4, pp. 3170–3180, Apr. 2021.

[34] C. She, Z. Wang, F. Sun, P. Liu, and L. Zhang, "Battery aging assessment for real-world electric buses based on incremental capacity analysis and radial basis function neural network," *IEEE Trans. Ind. Infor*., vol. 16, no. 5, pp. 3345–3354, May 2020.

[35] P. Shrivastava, T. Kok Soon, M. Y. I. Bin Idris, S. Mekhilef and S. B. R. S. Adnan, "Combined State of Charge and State of Energy Estimation of Lithium-Ion Battery Using Dual Forgetting Factor-Based Adaptive Extended Kalman Filter for Electric Vehicle Applications," in *IEEE Transactions on Vehicular Technology*, vol. 70, no. 2, pp. 1200-1215, Feb. 2021.

[36] Z. He, Z. Yang, X. Cui, and E. Li, "A Method of State-of-Charge Estimation for EV Power Lithium-Ion Battery Using a Novel Adaptive Extended Kalman Filter," in *IEEE Transactions on Vehicular Technology*, vol. 69, no. 12, pp. 14618-14630, Dec. 2020.

[37] X. Sun, J. Ji, B. Ren, C. Xie, and D. Yan, "Adaptive forgetting factor recursive least square algorithm for online identification of equivalent

circuit model parameters of a lithium-ion battery," *Energies*, vol. 12, no. 12, p. 2242, 2019.

[38] X. Lin, Y. Tang, J. Ren, and Y. Wei, "State of charge estimation with the adaptive unscented Kalman filter based on an accurate equivalent circuit model," *Journal of Energy Storage*, vol. 41, p. 102840, Sep. 2021.

[39] S. Marelli and M. Corno, "Model-based estimation of lithium concentrations and temperature in batteries using soft-constrained dual unscented Kalman filtering," *IEEE Transactions on Control Systems Technology*, vol. 29, no. 2, pp. 926–933, Mar. 2021.

[40] N. Peng, S. Zhang, X. Guo, and X. Zhang, "Online parameters identification and state of charge estimation for lithium-ion batteries using improved adaptive dual unscented Kalman filter," *International Journal of Energy Research*, vol. 45, no. 1, pp. 975–990, Oct. 2020.

[41] J. Feng, F. Cai, J. Yang, S. Wang, and K. Huang, "An Adaptive State of Charge Estimation Method of Lithium-ion Battery Based on Residual Constraint Fading Factor Unscented Kalman Filter," in *IEEE Access*, vol. 10, pp. 44549-44563, 2022.

[42] Liu, J. Wang, Q. Liu, J. Tang, H. Liu, and Z. Fang, "Deep-Discharging Li-Ion Battery State of Charge Estimation Using a Partial Adaptive Forgetting Factors Least Square Method," in *IEEE Access*, vol. 7, pp. 47339-47352, 2019.

[43] X. Yan, G. Zhou, W. Wang, P. Zhou and Z. He, "A Hybrid Data-Driven Method for State-of-Charge Estimation of Lithium-Ion Batteries," in IEEE Sensors Journal, vol. 22, no. 16, pp. 16263-16275, 15 Aug.15, 2022.

[44] G. S. Misyris, D. I. Doukas, T. A. Papadopoulos, D. P. Labridis and V. G. Agelidis, "State-of-Charge Estimation for Li-Ion Batteries: A More Accurate Hybrid Approach," in *IEEE Transactions on Energy Conversion*, vol. 34, no. 1, pp. 109-119, March 2019.

[45] B. Moulik, A. K. Dubey and A. M. Ali, "A Battery Modeling Technique Based on Fusion of Hybrid and Adaptive Algorithms for Real-Time Applications in Pure EVs," in *IEEE Transactions on Intelligent Transportation Systems*, vol. 24, no. 3, pp. 2760-2771, March 2023.

[46] Hongwen He, Rui Xiong, Xiaowei Zhang, Fengchun Sun, and JinXin Fan, "State-of-charge estimation of the lithium-ion battery using an adaptive extended Kalman filter based on an improved Thevenin model," *IEEE Transactions on Vehicular Technology*, vol. 60, no. 4, pp. 1461–1469, 2011.

[47] Z. Chen, Y. Fu, and C. C. Mi, "State of charge estimation of lithium-ion batteries in electric drive vehicles using extended Kalman filtering," *IEEE Transactions on Vehicular Technology*, vol. 62, no. 3, pp. 1020–1030, 2013.

[48] Q.-Z. Zhang, X.-Y. Wang, and H.-M. Yuan, "Estimation for SOC of li-ion battery based on two order RC Temperature Model," *2018 13th IEEE Conference on Industrial Electronics and Applications (ICIEA)*, 2018.

[49] D. Vila, E. Hornberger, and C. Toigo, "Machine learning based state-of-charge prediction of electrochemical green hydrogen production: Zink-zwischenschritt-elektrolyseur (ZZE)," *Energy and AI*, vol. 16, p. 100355, May 2024.

[50] E. Galiounas *et al.*, "Battery state-of-charge estimation using machine learning analysis of ultrasonic signatures," *Energy and AI*, vol. 10, p. 100188, Nov. 2022.

[51] H. E. Perez, X. Hu, S. Dey, and S. J. Moura, "Optimal charging of Li-ion batteries with coupled electro-thermal-aging dynamics," *IEEE Transactions on Vehicular Technology*, vol. 66, no. 9, pp. 7761–7770, Sep. 2017.

[52] X. Lin *et al.*, "A lumped-parameter electro-thermal model for cylindrical batteries," *Journal of Power Sources*, vol. 257, pp. 1–11, Jul. 2014.

[53] Muhammad Fikri Irsyad Mat Razi *et al.*, "A review of internal resistance and temperature relationship, state of health and thermal runaway for lithium-ion battery beyond normal operating condition," *Journal of Advanced Research in Fluid Mechanics and Thermal Sciences*, vol. 88, no. 2, pp. 123–132, Nov. 2021.

[54] Phil Weicker, A Systems Approach to Lithium-Ion Battery Management, *Artech*, 2013.

[55] Matthew Keyser; Gi-Heon Kim; Jeremy Neubauer; Ahmad Pesaran; Shriram Santhanagopalan; Kandler Smith, Design and Analysis of Large Lithium-Ion Battery Systems, *Artech*, 2014.

[56] J. Warner, *Handbook of Lithium-Ion Battery Pack Design: Chemistry, Components, Types, and Terminology*, Elsevier, 2015.

[57] A. Khalid *et al.*, "Comparison of kalman filters for state estimation based on computational complexity of Li-Ion Cells," *Energies*, vol. 16, no. 6, p. 2710, Mar. 2023.